NASA Technical Memorandum 106353
ICOMP–93–31

Least-Squares Finite Element Solutions for Three-Dimensional Backward-Facing Step Flow

Bo-Nan Jiang and Lin-Jun Hou
Institute for Computational Mechanics in Propulsion
Lewis Research Center
Cleveland, Ohio

and

Tsung-Liang Lin
Livermore Software Technology Corporation
Livermore, California

Prepared for the
Fifth International Symposium on Computational Fluid Dynamics
Sendai, Japan, August 31–September 3, 1993

NASA

LEAST-SQUARES FINITE ELEMENT SOLUTIONS FOR THREE-DIMENSIONAL BACKWARD-FACING STEP FLOW

Bo-Nan Jiang and Lin-Jun Hou

Institute for Computational Mechanics in Propulsion
NASA Lewis Research Center
Cleveland, OH 44135, USA

Tsung-Liang Lin

Livermore Software Technology Corporation, Livermore, CA 94550, USA

ABSTRACT

Comprehensive numerical solutions of the steady state incompressible viscous flow over a three-dimensional backward-facing step up to $Re = 800$ are presented. The results are obtained by the least-squares finite element method (LSFEM) which is based on the velocity-pressure-vorticity formulation. The computed model is of the same size as that of Armaly's experiment. Three dimensional phenomena are observed even at low Reynolds number. The calculated values of the primary reattachment length are in good agreement with experimental results.

1. INTRODUCTION

It is well known that for backward-facing step flows the reattachment length obtained by 2D calculations cannot match with the experimental results for $Re \geq 450$. All the deviations of two-dimensional simulations from experimental results are mainly due to the growing effects of three-dimensionality as Reynolds number increases. In recent years, the development of numerical schemes in fluid dynamics has been concentrated on the solution of three-dimensional problems. Ku *et al.*[1] applied a pseudospectral matrix element method to simulate the same three-dimensional problem only up to $Re = 450$ by employing the primitive variable formulation. A simplified marker-and-cell finite-difference scheme is applied by Ikohagi and co-workers[2] for the same 3D problem in curvilinear coordinates. However, no comparisons have been made with either the experimental data or other simulation results, and thus no primary conclusions can be really made.

In this paper, we report our results for the 3D backward-facing step flow, and compare with experimental results. We use the least-squares finite element method (LSFEM) [3,4,5]. For incompressible viscous flows, the LSFEM is based on the first-order velocity-pressure-vorticity formulation. This method uses C^0 elements to discretize the equations and minimizes the L_2 norm of the equation residuals, and results in a symmetric and positive-definite algebraic system which can be solved by simple matrix-free iterative methods. This method leads to a minimization problem, and the choice of elements are thus free of the limitation of the Ladyzhenskaya-Babuska-Brezzi(LBB) conditions[6]. The LSFEM is also free of any parameters. Furthermore, all unknown variables are solved in a fully coupled manner, and only simple physical boundary conditions are imposed, no artificial numerical boundary conditions need be devised.

2. VELOCITY-PRESSURE-VORTICITY FORMULATION

The mathematical formulation and numerical scheme of the LSFEM for 3D Navier-Stokes equations can be found in Jiang *et al.*[5]. For completeness, here we give a brief description of the method. The steady-state incompressible Navier-Stokes equations can be recast as the following nondimensional first-order quasi-linear velocity-pressure-vorticity formulation

$$\nabla \cdot \bar{\mathbf{u}} = 0, \qquad in\ \Omega, \tag{1}$$

$$\bar{\mathbf{u}} \cdot \nabla \bar{\mathbf{u}} + \nabla p + \frac{1}{Re} \nabla \times \bar{\omega} = \bar{f}, \qquad in\ \Omega, \tag{2}$$

$$\bar{\omega} - \nabla \times \bar{\mathbf{u}} = 0, \qquad in\ \Omega \tag{3}$$

in which $\bar{\mathbf{u}}$ denotes the velocity, p the pressure, $\bar{\mathbf{f}}$ the body force, Re the Reynolds number, and Ω the flow domain. Here an independent vector, the vorticity $\bar{\omega} = \nabla \times \bar{\mathbf{u}}$, is introduced to yield the first-order form such that the C^0 element can be used. As proved by Jiang *et*

al. [5], the following compatibility condition is required for three-dimensional cases to make the system elliptic and will not be detailed here,

$$\nabla \cdot \bar{\omega} = 0. \tag{4}$$

The first-order elliptic system in Cartesian coordinates for three-dimensional problems can be expressed as

$$\begin{aligned}
\frac{\partial u}{\partial x} + \frac{\partial v}{\partial y} + \frac{\partial w}{\partial z} &= 0 \\
u\frac{\partial u}{\partial x} + v\frac{\partial u}{\partial y} + w\frac{\partial u}{\partial z} + \frac{\partial p}{\partial x} + \frac{1}{Re}(\frac{\partial \omega_z}{\partial y} - \frac{\partial \omega_y}{\partial z}) &= f_x \\
u\frac{\partial v}{\partial x} + v\frac{\partial v}{\partial y} + w\frac{\partial v}{\partial z} + \frac{\partial p}{\partial y} + \frac{1}{Re}(\frac{\partial \omega_x}{\partial z} - \frac{\partial \omega_z}{\partial x}) &= f_y \\
u\frac{\partial w}{\partial x} + v\frac{\partial w}{\partial y} + w\frac{\partial w}{\partial z} + \frac{\partial p}{\partial z} + \frac{1}{Re}(\frac{\partial \omega_y}{\partial x} - \frac{\partial \omega_x}{\partial y}) &= f_z \\
\omega_x + \frac{\partial v}{\partial z} - \frac{\partial w}{\partial y} &= 0 \\
\omega_y + \frac{\partial w}{\partial x} - \frac{\partial u}{\partial z} &= 0 \\
\omega_z + \frac{\partial u}{\partial y} - \frac{\partial v}{\partial x} &= 0 \\
\frac{\partial \omega_x}{\partial x} + \frac{\partial \omega_y}{\partial y} + \frac{\partial \omega_z}{\partial z} &= 0
\end{aligned} \tag{5}$$

This first-order system has seven unknowns and eight equations. Jiang[5] proved that the system is determined by introducing a dummy variable ϕ which satisfies the boundary condition $\phi = 0$ on the boundary. The gradient, $\nabla\phi$, is then added to the equation of vorticity definition, and thus yields an elliptic and determined system with eight unknowns and eight equations. Taking divergence of this vorticity equation will lead to $\Delta\phi = 0$, thus $\phi \equiv 0$ in Ω. Note that the introduction of a dummy variable ϕ is purely for the purpose of proving the ellipticity of the system (5). In real calculation, no extra unknown is needed.

As shown in Jiang *et al.* [5], the 3D incompressible Navier-Stokes equations must have three boundary conditions on each boundary. For the backward-facing step flow problem, the following boundary conditions are considered :

(a) $u = v = w = 0$ on the wall;

(b) $u = specified$, $v = w = 0$ at the well-developed inflow;

(c) $v = w = 0$, $p = constant$ (reference) at the outflow;

(d) $\omega_x = \omega_y = 0$, $w = 0$ at the symmetric plane.

Note that no derivatives are involved in the boundary conditions, only the simple physical boundary conditions are imposed, and vorticity boundary conditions are used only at the symmetric plane.

3. NUMERICAL SCHEME

First, the Newton's scheme is employed to linearize the quasi-linear system, thus we have, for example,

$$u\frac{\partial u}{\partial x} \approx u^{o}\frac{\partial u}{\partial x} + u(\frac{\partial u}{\partial x})^{o} - u^{o}(\frac{\partial u}{\partial x})^{o} \tag{6}$$

where $(\,)^{o}$ denotes the evaluation of the variable from previous iteration level. Then the linearized first-order equations can be written as a standard first-order system

$$\mathbf{L}\,\mathbf{u} = \mathbf{f} \quad in\ \Omega \tag{7}$$

where $\mathbf{L}$ is a first-order partial differential operator :

$$\mathbf{L}\,\mathbf{u} = \mathbf{A_1}\frac{\partial \mathbf{u}}{\partial x} + \mathbf{A_2}\frac{\partial \mathbf{u}}{\partial y} + \mathbf{A_3}\frac{\partial \mathbf{u}}{\partial z} + \mathbf{A}\,\mathbf{u} \tag{8}$$

The coefficient matrices in the general form of the first-order system for three-dimensional problems are

$$\mathbf{A}_1 = \begin{bmatrix} 1 & 0 & 0 & 0 & 0 & 0 & 0 \\ u^{o} & 0 & 0 & 1 & 0 & 0 & 0 \\ 0 & u^{o} & 0 & 0 & 0 & 0 & \frac{-1}{Re} \\ 0 & 0 & u^{o} & 0 & 0 & \frac{1}{Re} & 0 \\ 0 & 0 & 0 & 0 & 0 & 0 & 0 \\ 0 & 0 & 1 & 0 & 0 & 0 & 0 \\ 0 & -1 & 0 & 0 & 0 & 0 & 0 \\ 0 & 0 & 0 & 0 & 1 & 0 & 0 \end{bmatrix}, \quad \mathbf{A}_2 = \begin{bmatrix} 0 & 1 & 0 & 0 & 0 & 0 & 0 \\ v^{o} & 0 & 0 & 0 & 0 & 0 & \frac{1}{Re} \\ 0 & v^{o} & 0 & 1 & 0 & 0 & 0 \\ 0 & 0 & v^{o} & 0 & \frac{-1}{Re} & 0 & 0 \\ 0 & 0 & -1 & 0 & 0 & 0 & 0 \\ 0 & 0 & 0 & 0 & 0 & 0 & 0 \\ 1 & 0 & 0 & 0 & 0 & 0 & 0 \\ 0 & 0 & 0 & 0 & 0 & 1 & 0 \end{bmatrix} \tag{9}$$

$$\mathbf{A}_3 = \begin{bmatrix} 0 & 0 & 1 & 0 & 0 & 0 & 0 \\ w^{o} & 0 & 0 & 0 & 0 & \frac{-1}{Re} & 0 \\ 0 & w^{o} & 0 & 0 & \frac{1}{Re} & 0 & 0 \\ 0 & 0 & w^{o} & 1 & 0 & 0 & 0 \\ 0 & 1 & 0 & 0 & 0 & 0 & 0 \\ -1 & 0 & 0 & 0 & 0 & 0 & 0 \\ 0 & 0 & 0 & 0 & 0 & 0 & 0 \\ 0 & 0 & 0 & 0 & 0 & 0 & 1 \end{bmatrix}, \quad \mathbf{A} = \begin{bmatrix} 0 & 0 & 0 & 0 & 0 & 0 & 0 \\ (\frac{\partial u}{\partial x})^{o} & (\frac{\partial u}{\partial y})^{o} & (\frac{\partial u}{\partial z})^{o} & 0 & 0 & 0 & 0 \\ (\frac{\partial v}{\partial x})^{o} & (\frac{\partial v}{\partial y})^{o} & (\frac{\partial v}{\partial z})^{o} & 0 & 0 & 0 & 0 \\ (\frac{\partial w}{\partial x})^{o} & (\frac{\partial w}{\partial y})^{o} & (\frac{\partial w}{\partial z})^{o} & 0 & 0 & 0 & 0 \\ 0 & 0 & 0 & 0 & 1 & 0 & 0 \\ 0 & 0 & 0 & 0 & 0 & 1 & 0 \\ 0 & 0 & 0 & 0 & 0 & 0 & 1 \\ 0 & 0 & 0 & 0 & 0 & 0 & 0 \end{bmatrix} \tag{10}$$

and the force and state variable vectors are

$$\mathbf{f} = \begin{Bmatrix} 0 \\ u^o(\frac{\partial u}{\partial x})^o + v^o(\frac{\partial u}{\partial y})^o + w^o(\frac{\partial u}{\partial z})^o \\ u^o(\frac{\partial v}{\partial x})^o + v^o(\frac{\partial v}{\partial y})^o + w^o(\frac{\partial v}{\partial z})^o \\ u^o(\frac{\partial w}{\partial x})^o + v^o(\frac{\partial w}{\partial y})^o + w^o(\frac{\partial w}{\partial z})^o \\ 0 \\ 0 \\ 0 \\ 0 \end{Bmatrix}, \qquad \mathbf{u} = \begin{Bmatrix} u \\ v \\ w \\ p \\ \omega_x \\ \omega_y \\ \omega_z \end{Bmatrix} \tag{11}$$

The linearized first-order equations are solved by the LSFEM [3] which results in a symmetric and positive-definite algebraic equation. A Jacobi preconditioned conjugate gradient method is employed to solve the linear algebraic equations. In the conjugate gradient method, the major computation is the multiplication of the global matrix with the global vector, and this can be done in an element-by-element manner without forming the global matrix[7]. To further save the storage, the current algorithm does not even form the element matrices. We directly calculate the product of the element matrix and the element vector, and the Jacobi preconditioner can also be easily formed at the same time. In this way, we store only several global vectors, and the derivatives of the shape functions at Gaussian points for each element.

4. NUMERICAL RESULTS

The geometry and boundary conditions for the 3D model are shown in Figure 1. Due to the symmetry, only half of the domain is considered. The step has a height S=4.9 mm, and the inlet boundary is located 3.5 step heights upstream of this step. The channel downstream of the step has a height of 10.1 mm that provides an expansion ratio of 1 : 1.9423, and the half-span $W = 90\,mm$ that provides an aspect ratio for the test channel is 18 : 1.01. The length L measured from the step to the end of the calculation domain is 45 step heights, which is 3.11 times the maximum experimentally measured reattachment length of the primary recirculation region for the Renolds numbers interested. The Reynolds number $Re = UD/\nu$ is based on the hydraulic diameter ($D = 10.4\,mm$) of the inlet channel, and the average velocity is two-thirds of the maximum inlet velocity (normalized to unity) on the mid-span plane. The various Reynolds numbers are obtained by varying the kinematic viscosity ν. The velocity profiles obtained by solving the 2D Poisson's equation for a well-developed flow are imposed as the inflow boundary conditions. The outflow boundary conditions are defined such that a parallel flow and a constant pressure field exist.

The computation was performed on the mesh with 54400 nonuniform trilinear elements ($6 \times 16 \times 20$ for inlet channel and $82 \times 32 \times 20$ for the test channel). The smallest element has the size of 0.1251, 0.05714 and 0.421 steps in x, y and z direction individually, while the

largest element has the size of 3.0, 0.06938 and 1.68367 steps respectively. Figure 2 shows the nonuniform mesh which has more elements close to the sidewall, the floor and the roof in the test channel (see Figure 2). The solutions of the Stokes problem are taken as initial guesses for the case of $Re = 100$, and the "converged" solutions are then used as initial guesses for higher Reynolds numbers. The "converged" solutions are based on those whose L_2 norm of the residuals less than 1.0×10^{-4}. The problem is solved using about $5M$ words of the memory on a CRAY-YMP. Simulation of the three-dimensional model is performed from $Re = 100$ to 800.

Spanwise flow structure

The velocity profiles at three spanwise locations for $Re = 277$ and 800 are shown in Figures 3 and 5. At $Re = 277$, there is a slight change in the spanwise flow structure and reattachment length. At $Re = 800$, the velocity profiles change significantly in spanwise direction, and the reattachment length increases rapidly as moving toward the mid-plane. Figures 4 and 6 depict the pressure contours at these two Reynolds numbers. Again, the change in spanwise pressure distribution is more obvious as Reynolds number increases. Most researchers predicted the reattachment length well up to $Re \leq 450$ by their 2D simulations, and thought that the two-dimensional phenomena were maintained until $Re \approx 450$. Numerical results from the present method, however, show that the three-dimensionality are quite significant even at low Reynolds number (e.g. Re=277).

Figure 7 illustrates the contours of vorticity ω_x from $z = 6.5\,cm$ to the sidewall ($z = 9.0\,cm$) at $Re = 277$. The dashed lines indicate the negative contour values. As shown in the Figures, the vortex is stronger near the sidewall and has negligible influence on the region near the mid-plane. The study of velocity vectors along the span at different downstream locations provides better view of the three-dimensional phenomena, see Figure 8. The behaviour of the inward flow toward the mid-span at the top roof and the outward flow toward the sidewall ($z/W = 1.0$) at the channel floor contributes the three-dimensional phenomena. This three-dimensionality around the corner of the sidewall and the step can also be found at lower Reynolds numbers but less significant.

A series of plots of cross-flow velocity vectors and contours of streamwise vorticity, ω_x, at different downstream locations are shown in Figures 9 - 14. At $Re = 389$, there is a counter-clockwise (negative) vortex on the corner of sidewall and channel floor. The cross-flow velocity vectors shown in Figure 10 depict that there is a weaker clockwise (positive) vortex close to the channel ceiling as flow moving downstream. The size of this positive vortex grows in the streamwise direction. Both vortexes become stronger as Reynolds number increases, and persist further downstream with decreasing strength.

It is found that except in the inlet channel and in the region which is very far downstream of the step, the three-dimensionality is significant at the downstream, in the vicinity of the step. A study of spanwise flow structure provides further details. The spanwise distribution of velocity profiles for streamwise velocity, u, at various x-locations and at a fixed y-position

for $Re = 648$ are shown in Figure 15. At $y = 7.5\,mm$, all velocity profiles close to the mid-plane are basically two-dimensional. The negative velocities in the figure indicate that a second separation bubble occurs on the ceiling, and its thickness grows as close to the sidewall. At $y = 2.35\,mm$, the x-component velocity, u, first increases rapidly in about the thickness of boundary layer, then drops and resumes two-dimensional flow from $z/W = 0.5$ to the mid-plane ($z/W = 0.0$).

Figure 16 demonstrates the three-dimensionality by depicting the spanwise distribution of the reattachment length for the primary separated-flow region. The numerical data of spanwise reattachment length vs. various Reynolds numbers are listed in Table 1. The reattachment length is pretty much constant close to the mid-plane and decreases as moving toward the sidewall. It is interesting to note that next to the sidewall, the reattachment length increases rapidly. This phenomenon might be due to the interaction of primary recirculation vortex and the corner vortex between the sidewall and floor as shown in, for example, Figures 9 and 10. Figure 17 shows the computed reattachment length of the primary recirculation zone, and compares with Armaly *et al.*'s[8] experimental results. The corresponding pointwise data obtained by the LSFEM and the experiment are given in Table 2. Since no tabular results are given, here the cited data from experiment are obtained by optically digitizing Figure 14 in Armaly *et al.*'s paper.

Table 2 shows that in the Re range for which most simulations fail to predict the reattachment length because of the three-dimensional phenomenon ($Re = 450 \sim 800$), the calculated results by the LSFEM agree very well with the experimental results up to $Re = 800$.

As Reynolds number increases, an additional separated-flow region occurs near the channel ceiling. Figure 18 illustrates the spanwise detachment (x_4/S) and reattachment (x_5/S) lines of this second eddy. The present results show that as Reynolds number increases, this upper-wall eddy propagates toward the mid-plane with its length decreasing toward the mid-plane. For example, as Reynolds number increases from 600 to 800, its length changes from 17.5 to 22 step heights at $z/W = 0.97708$, and changes from 0.2 to 9.36 step heights at $z/W = 0.76$. The experimentally observed upper-wall eddy at the mid-plane was not observed in the current simulation. The spanwise variation of detachment and reattachment length of the second eddy for various Reynolds numbers are given in Tables 3 and 4.

5. CONCLUSIONS

The steady-state three-dimensional backward-facing step problem is simulated using the least-squares finite element method. The computed spanwise flow structure clearly depicts the three-dimensionality. The prediction of primary reattachment length are in good agreement with experimental results. Further developments are under way for solving time-dependent problems.

REFERENCES

1. H. C. Ku, R. S. Hirsh, T. D. Taylor and A. P. Rosenberg, "A Pseudospectral Matrix Element for Solution of Three-Dimensional Incompressible Flows and Its Parallel Implementation," *J. Comp. Phys.*, Vol. 83, 1989, pp. 260-291.

2. T. Ikohagi, B. R. Shin and H. Daiguji, "Application of an Implicit Time-Marching Scheme to a Three-Dimensional Incompressible Flow Problem in Curvilinear Coordinate Systems," *Computer Fluids*, Vol. 21, No. 2, 1992, pp.163-175.

3. B. N. Jiang and L. A. Povinelli, "Least-Squares Finite Element Method for Fluid Dynamics," *Comput. Meth. Appl. Mech. Eng.*, Vol. 81, 1990, pp.13-37.

4. B. N. Jiang, "A Least-Squares Finite Element Method for Incompressible Navier-Stokes Problems," *Inter. J. Numer. Meth. Fluids*, Vol. 14, 1992, pp.843-859.

5. B. N. Jiang, T. L. Lin and L. A. Povinelli, "Large-scale Computation of Incompressible Viscous Flow by Least-Squares Finite Element Method," submitted to *Computer Method in Apllied Mechanics and Engineering*, or see NASA TM 105904, ICOMP-93-06.

6. J. T. Oden and G. F. Carey, *Finite Elements: Mathematical Aspects, Vol.IV "*, Pretice-Hall, Englewood Cliffs, NJ, 1983.

7. G. F. Carey and B. N. Jiang, "Element-by-Element Linear and Nonlinear Solution Schemes," *Communications in Applied Numerical Methods*, Vol. 2, 1986, pp. 145-153.

8. B. F. Armaly, F. Durst, J. C. F. Pereira and B. Schonung, "Experimental and Theoretical Investigation of Backward-Facing Step Flow," *J. Fluid Mech.*, Vol. 127, 1982, pp.473-496.

Table 1. Spanwise Distribution of Primary Reattachment Length (x_1/S)

z/W	Re=389	Re=500	Re=600	Re=648	Re=700	Re=800
0.97708	4.7873	4.7598	4.8502	4.7166	4.8231	4.7052
0.95243	4.5224	4.5636	4.5934	4.5244	4.5810	4.5098
0.92591	4.4467	4.4700	4.4290	4.3849	4.3936	4.3248
0.89739	4.8376	4.7809	4.6438	4.5963	4.5364	4.4150
0.86670	5.6686	5.5985	5.4196	5.3551	5.2089	5.0171
0.83370	6.5050	6.6123	6.5767	6.5552	6.4553	6.2616
0.79819	6.9495	7.2317	7.3644	7.3418	7.4005	7.4756
0.76000	7.2835	7.6769	7.8567	7.7813	7.8771	7.9793
0.71892	7.6081	8.2233	8.4387	8.2980	8.4029	8.4371
0.67472	7.8156	8.8039	9.1300	8.9540	9.0833	8.9984
0.62719	7.9101	9.3172	9.8642	9.7360	9.8871	9.6695
0.57605	7.9336	9.6589	10.5745	10.6628	10.8592	10.6415
0.52104	7.9291	9.7898	11.0796	11.5275	11.8613	11.9200
0.46187	7.9188	9.8100	11.3667	12.1405	12.7017	13.3638
0.39823	7.9056	9.7822	11.4917	12.4468	13.2472	14.7292
0.32976	7.8933	9.7539	11.5069	12.4740	13.4493	15.5563
0.25611	7.8839	9.7385	11.4735	12.3895	13.4234	15.6984
0.17689	7.8780	9.7272	11.4279	12.3410	13.3384	15.4442
0.09167	7.8748	9.7209	11.4000	12.3408	13.2772	15.1296
0.00000	7.8740	9.7186	11.3926	12.3450	13.2504	15.0204

Table 2. Primary Reattachment Length (x_1/S)

Re	389	500	600	648	700	800
LSFEM	7.874	9.719	11.393	12.345	13.253	15.020
Exp.	8.67	10.21	11.40	12.36	13.10	14.45

Table 3. Detachment Length (x_4/S) of Secondary Eddy at Upper Wall

z/W	Re=389	Re=500	Re=600	Re=648	Re=700	Re=800
0.97708	3.0831	3.0024	2.8182	2.8258	2.7367	2.6701
0.95243	4.2783	4.1200	3.8681	3.8440	3.7324	3.6367
0.92591	5.6721	5.2026	4.9072	4.7961	4.6904	4.5429
0.89739	7.8333	6.1612	5.7713	5.5829	5.5169	5.3662
0.86670	–	7.3190	6.6515	6.3569	6.3083	6.1724
0.83370	–	–	7.6409	7.2013	7.1027	6.9149
0.79819	–	–	9.0375	8.2846	8.0603	7.6900
0.76000	–	–	11.3750	9.6379	9.3417	8.7960
0.71892	–	–	–	10.7500	10.5547	10.0307
0.67472	–	–	–	–	11.9552	11.0541
0.62719	–	–	–	–	–	12.2672
0.57605	–	–	–	–	–	14.1967

Table 4. Reatachment Length (x_5/S) of Secondary Eddy at Upper Wall

z/W	Re=389	Re=500	Re=600	Re=648	Re=700	Re=800
0.97708	13.7775	17.2220	20.3110	21.1037	22.7215	24.6619
0.95243	13.3167	17.0891	20.0150	20.9073	22.5413	24.2501
0.92591	12.2407	16.7674	19.6285	20.9271	22.4388	24.6982
0.89739	9.3224	15.3696	18.3668	19.9921	21.4839	24.0531
0.86670	–	12.8966	16.5111	17.8685	19.5302	22.0990
0.83370	–	–	14.7052	15.9967	17.7279	19.8740
0.79819	–	–	13.3818	14.9380	16.7597	18.4722
0.76000	–	–	11.5714	14.5169	16.1456	18.1593
0.71892	–	–	–	14.1530	15.7025	18.3837
0.67472	–	–	–	–	14.8041	18.5512
0.62719	–	–	–	–	–	18.1801
0.57605	–	–	–	–	–	16.7677

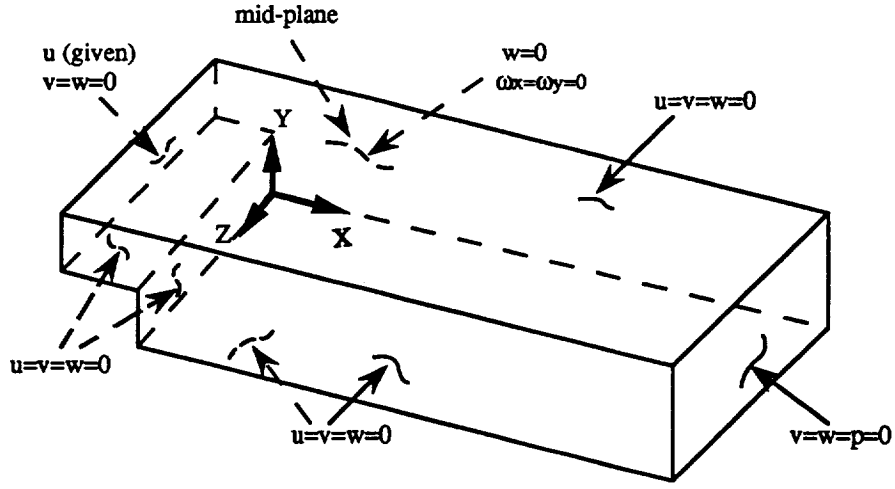

Figure 1. Backward-facing step geometry and boundary conditions.

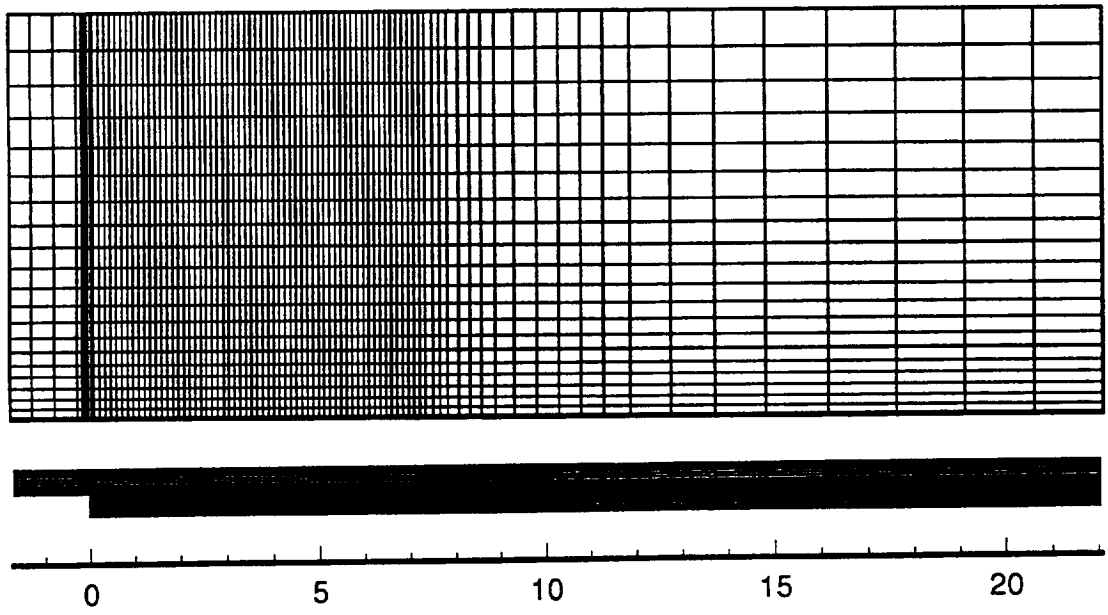

Figure 2. Nonuniform mesh (xy plane and xz plane).

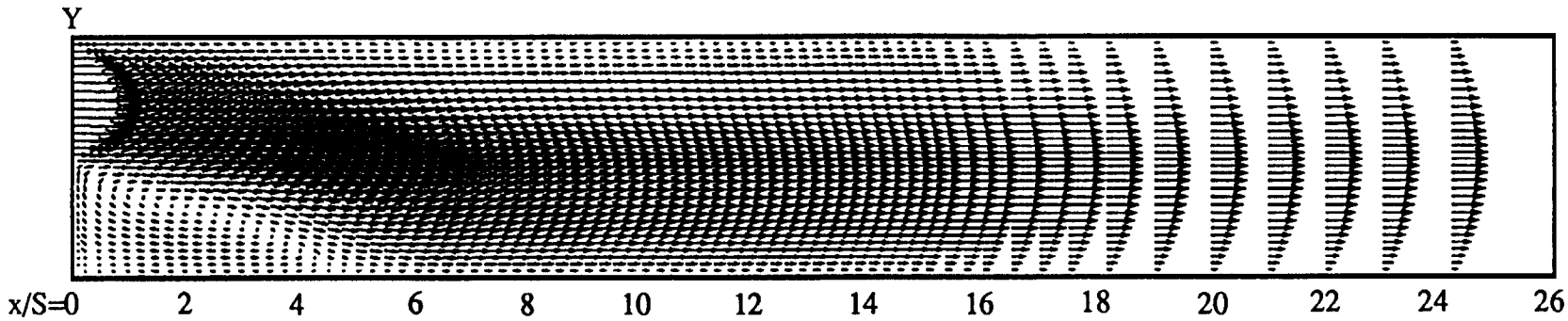

(a) z/W=0.8974

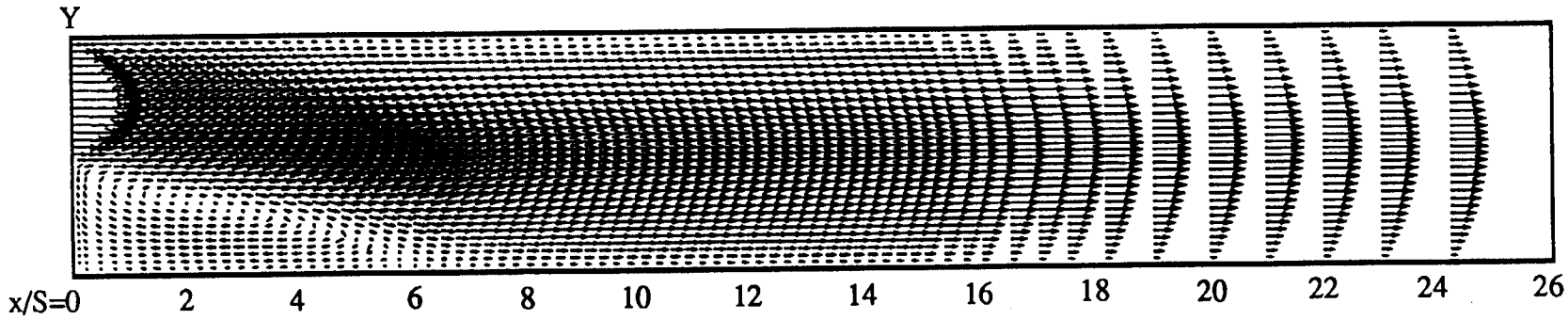

(b) z/W=0.76

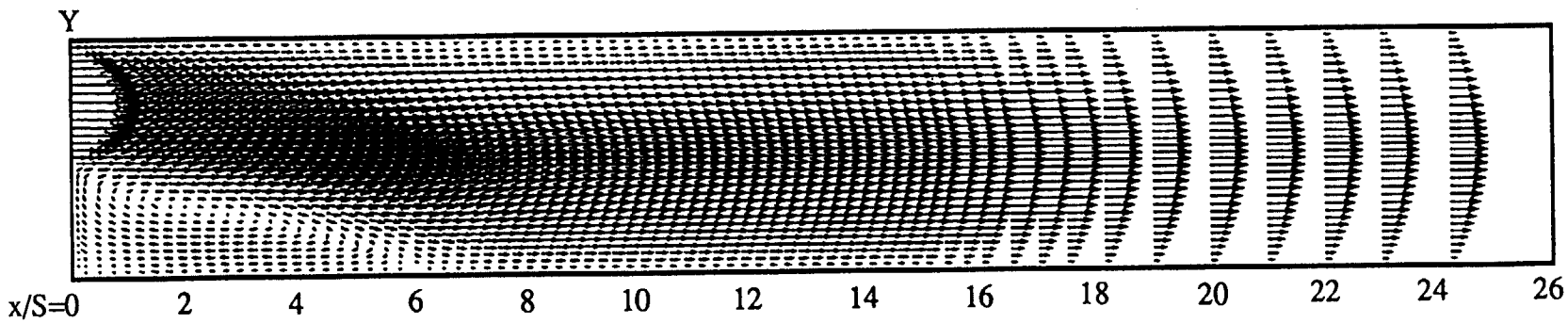

(c) z/W=0.0 (mid-plane)

Figure 3. Velocity profiles for Re=277.

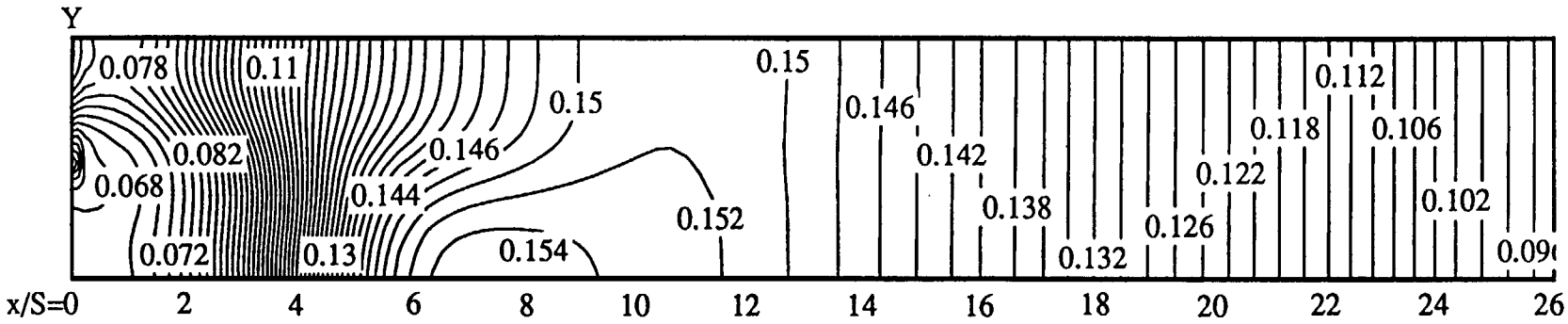

(a) z/W=0.8974

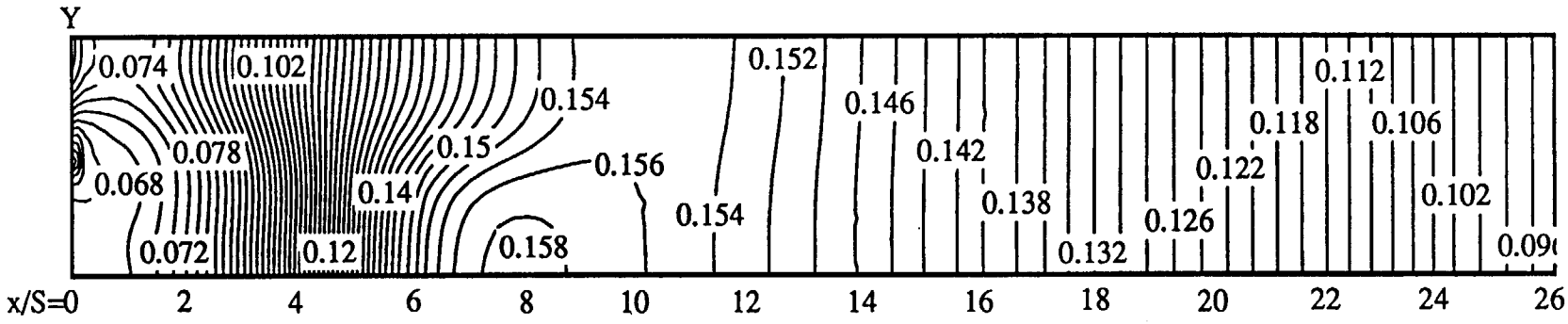

(b) z/W=0.76

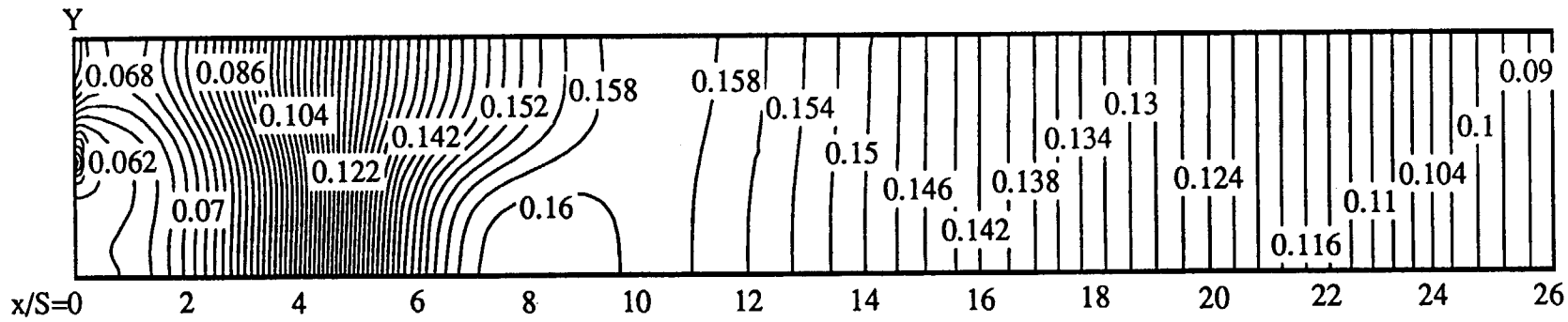

(c) z/W=0.0 (mid-plane)

Figure 4. Pressure contours for Re=277.

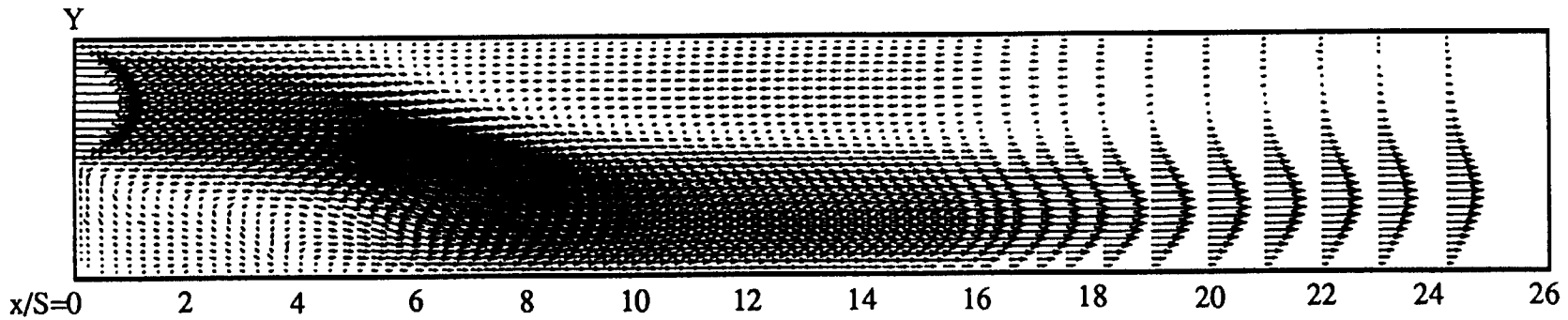

(a) z/W=0.8974

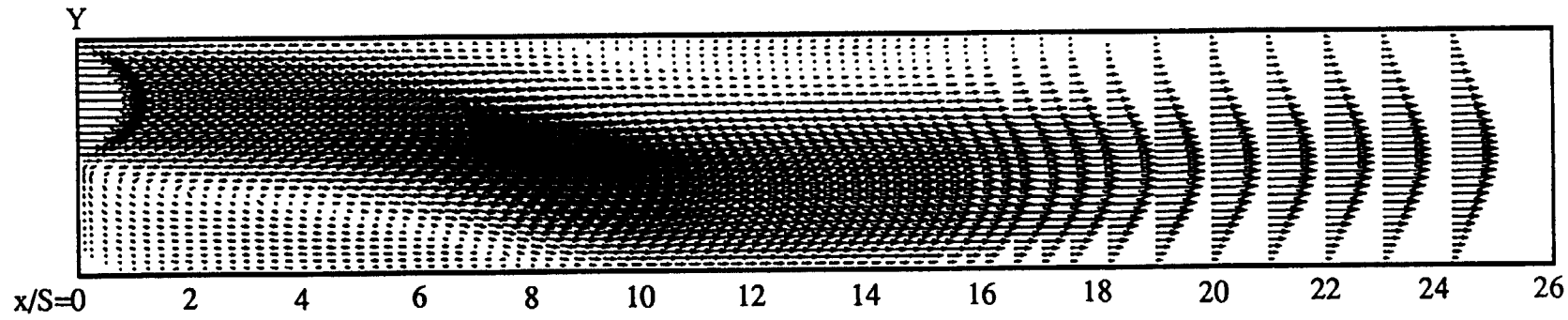

(b) z/W=0.76

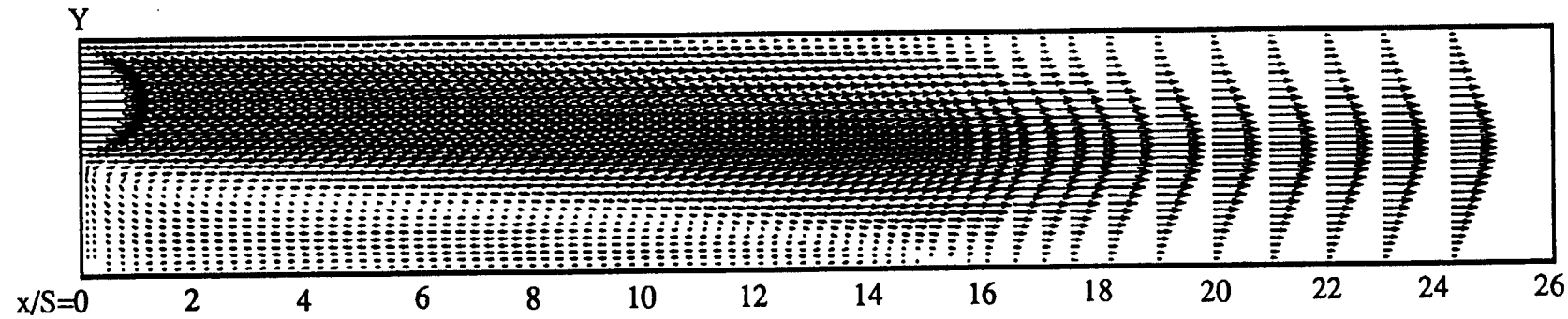

(c) z/W=0.0 (mid-plane)

Figure 5. Velocity profiles for Re=800.

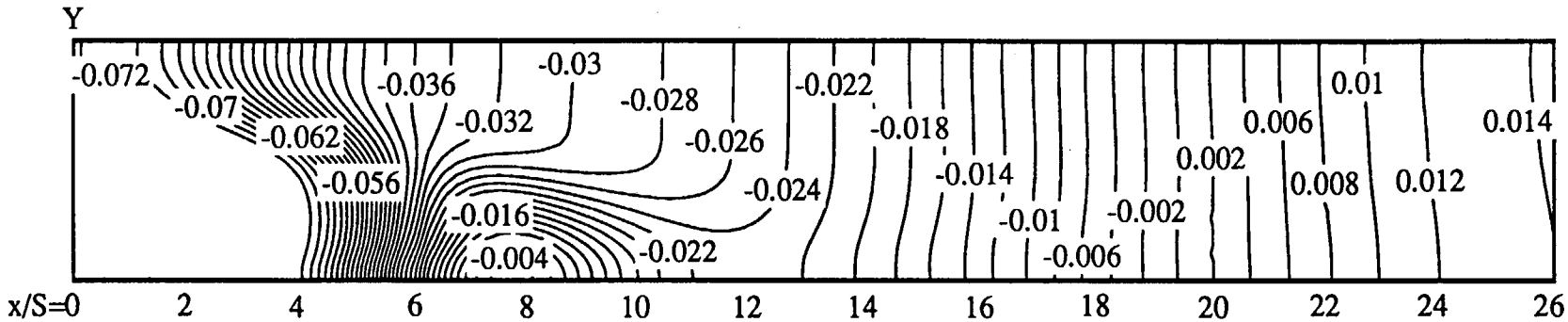

(a) z/W=0.8974

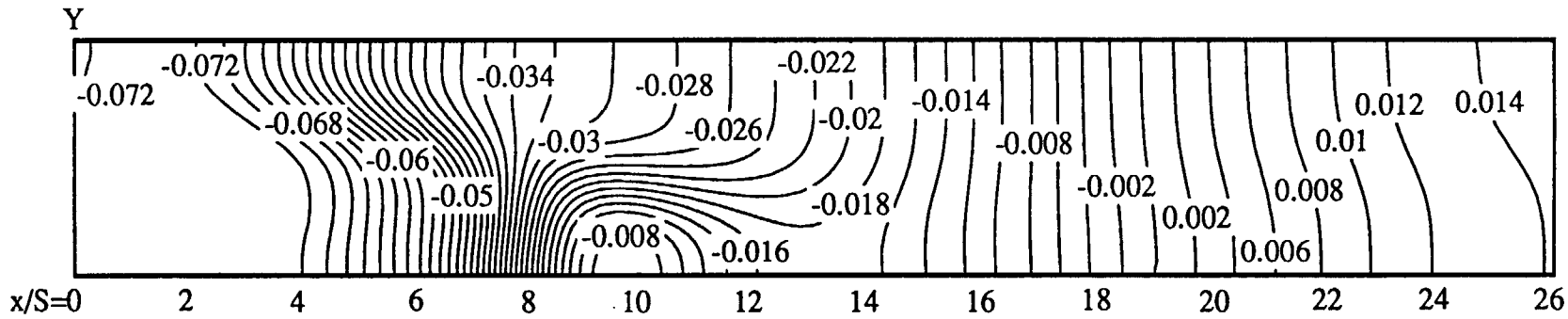

(b) z/W=0.76

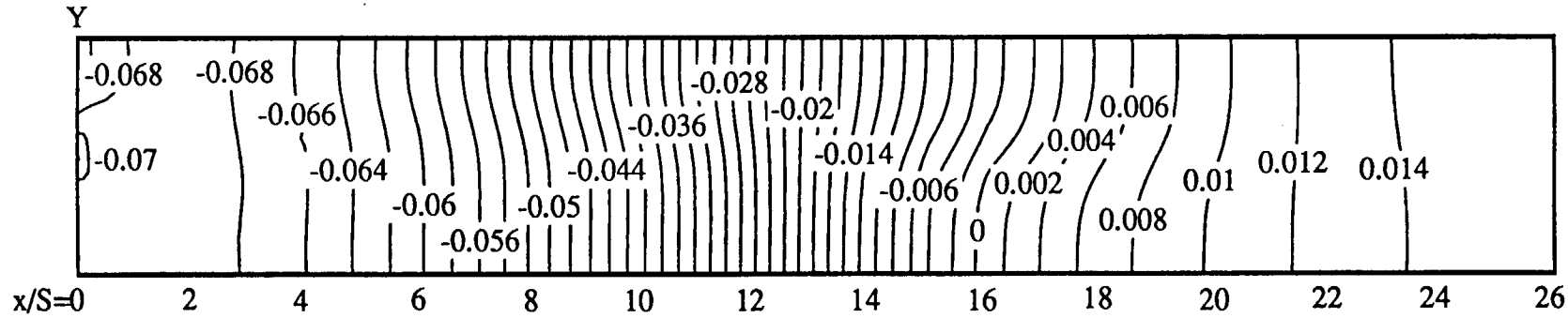

(c) z/W=0.0 (mid-plane)

Figure 6. Pressure contours for Re=800.

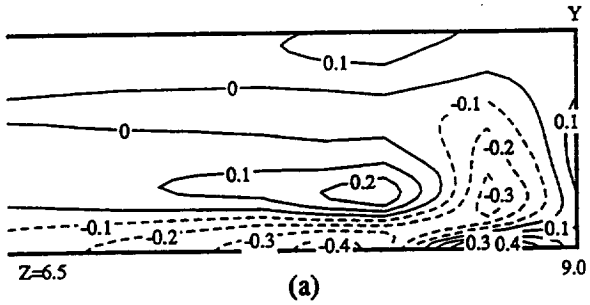

(a)

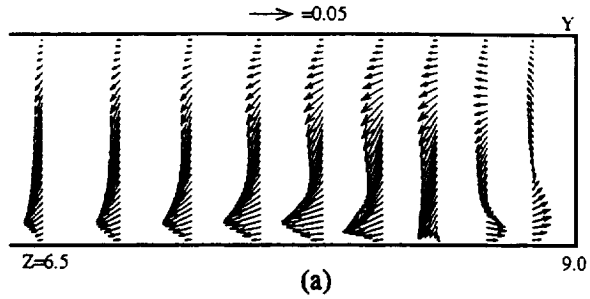

(a)

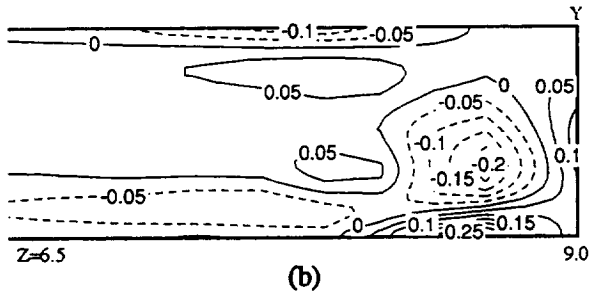

(b)

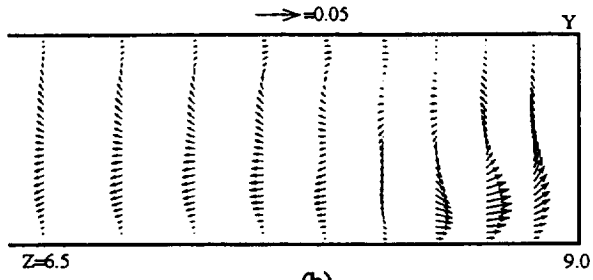

(b)

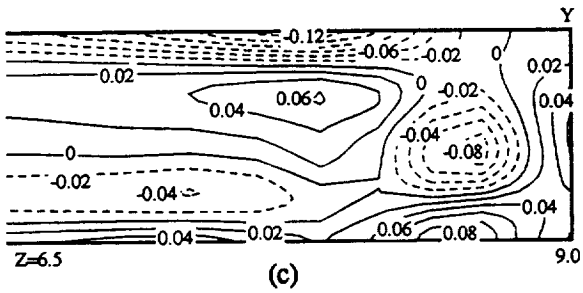

(c)

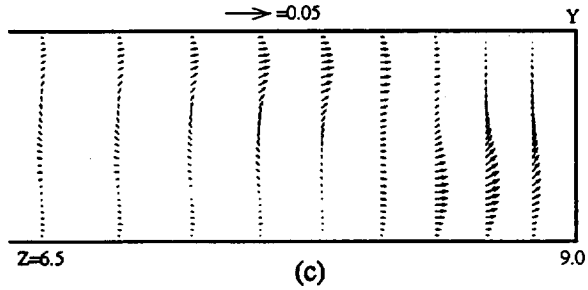

(c)

Figure 7. ωx contours for Re=277 at x/S= (a) 6.25, (b) 9.0, (c) 12.25.

Figure 8. Velocity vectors for Re=277 at x/S= (a) 6.25, (b) 9.0, (c) 12.25.

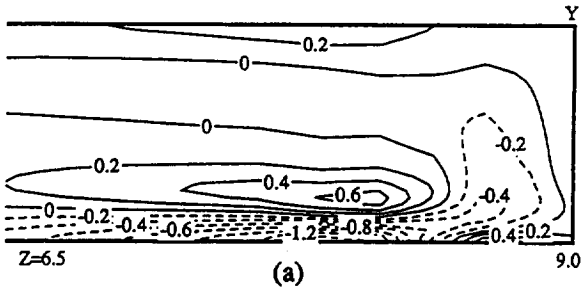

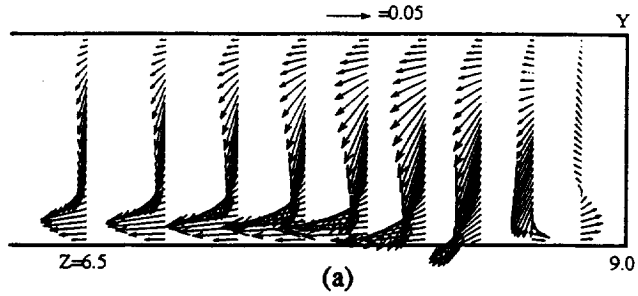

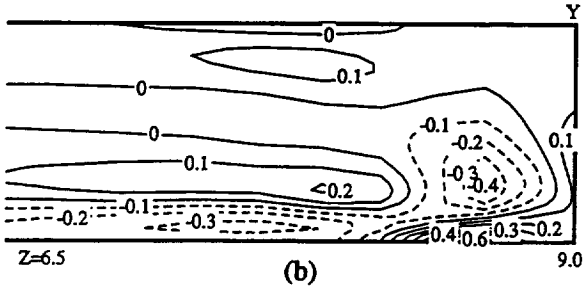

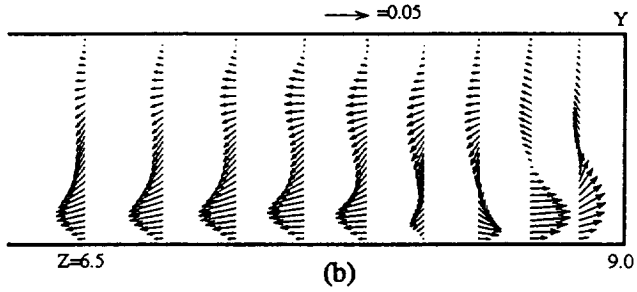

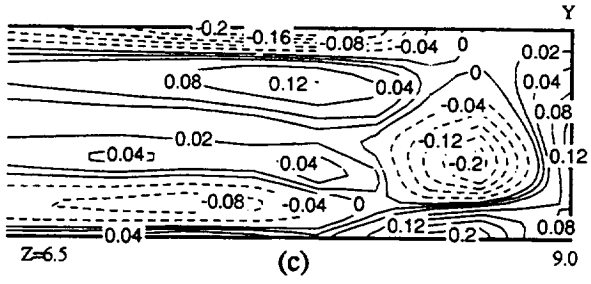

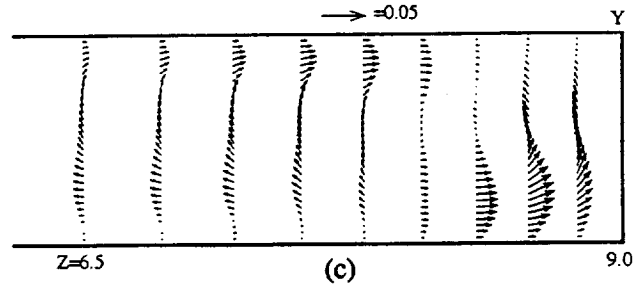

Figure 9. ωx contours for Re=389 at x/S= (a) 6.25, (b) 9.0, (c) 12.25.

Figure 10. Velocity vectors for Re=389 at x/S= (a) 6.25, (b) 9.0, (c) 12.25.

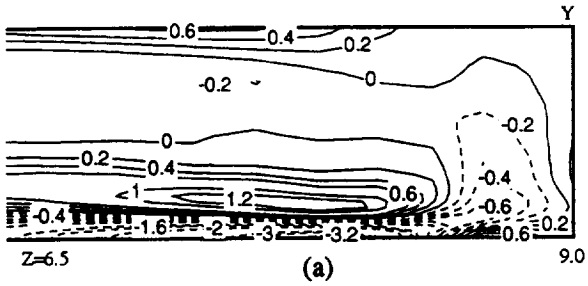

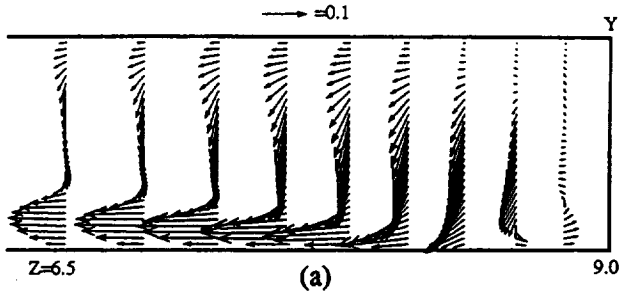

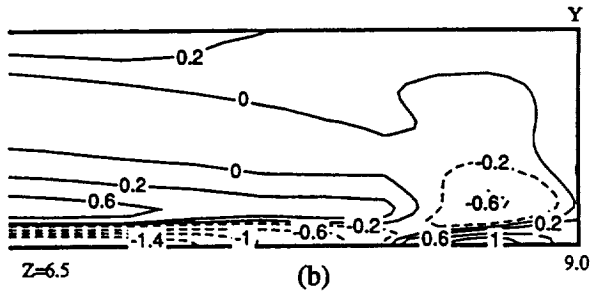

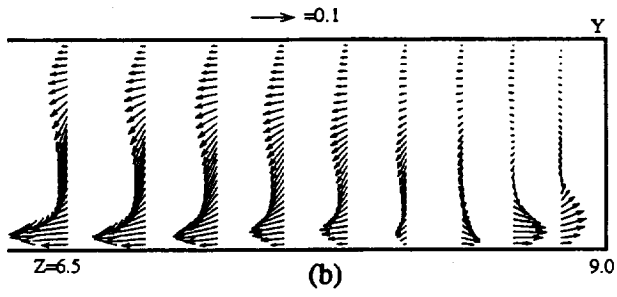

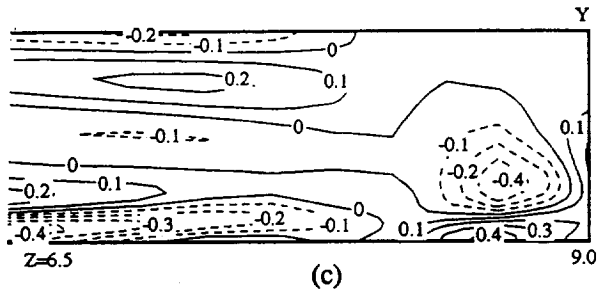

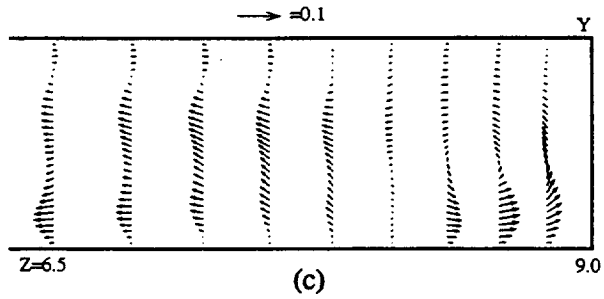

Figure 11. ωx contours for Re=648 at x/S= (a) 6.25, (b) 9.0, (c) 12.25.

Figure 12. Velocity vectors for Re=648 at x/S= (a) 6.25, (b) 9.0, (c) 12.25.

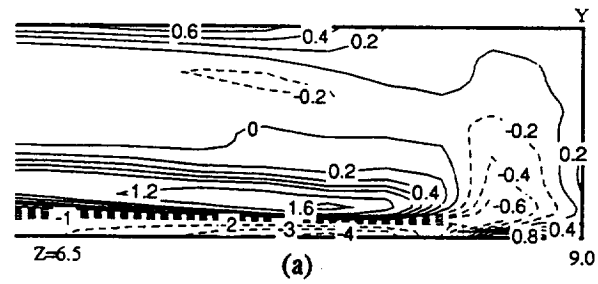

(a)

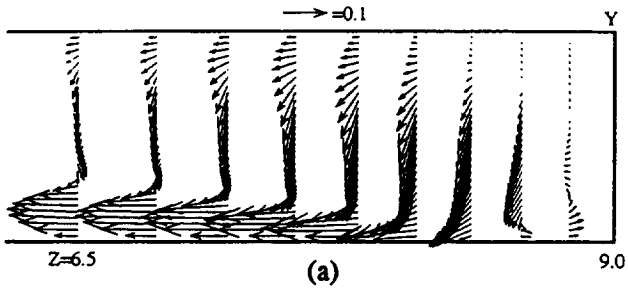

(a)

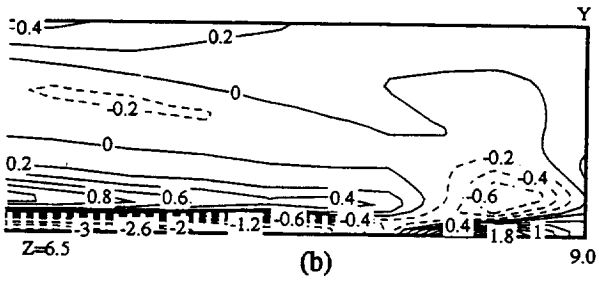

(b)

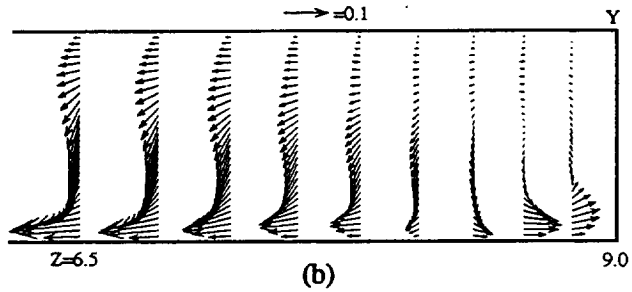

(b)

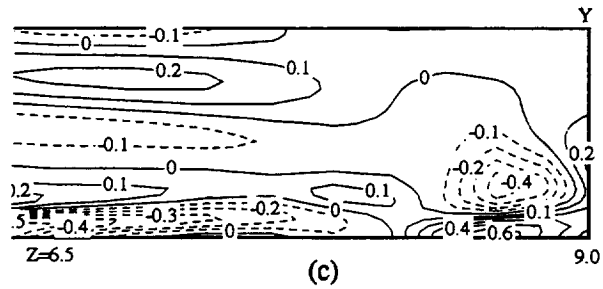

(c)

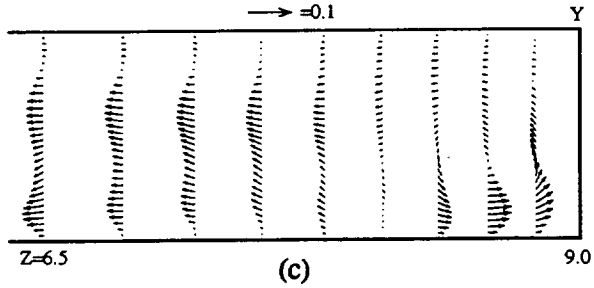

(c)

Figure 13. ω_x contours for Re=800 at x/S= (a) 6.25, (b) 9.0, (c) 12.25.

Figure 14. Velocity vectors for Re=800 at x/S= (a) 6.25, (b) 9.0, (c) 12.25.

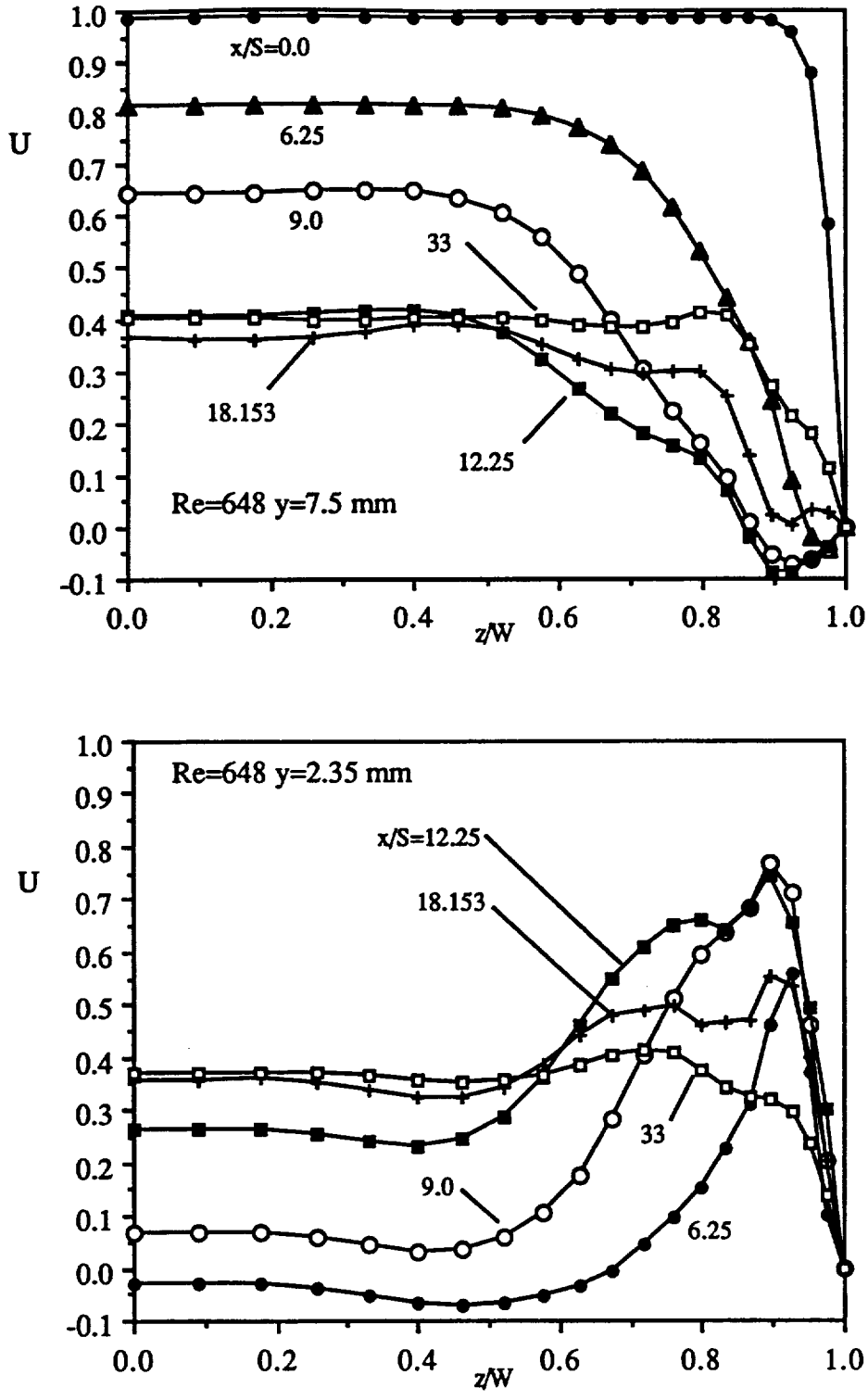

Figure 15. Spanwise distributions of U velocity profiles for Re=648.

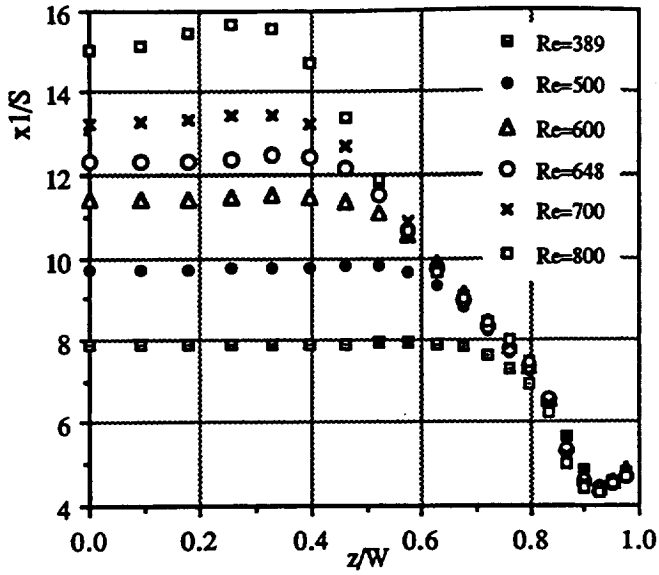

Figure 16. Spanwise locations of reattachment line for various Reynolds numbers.

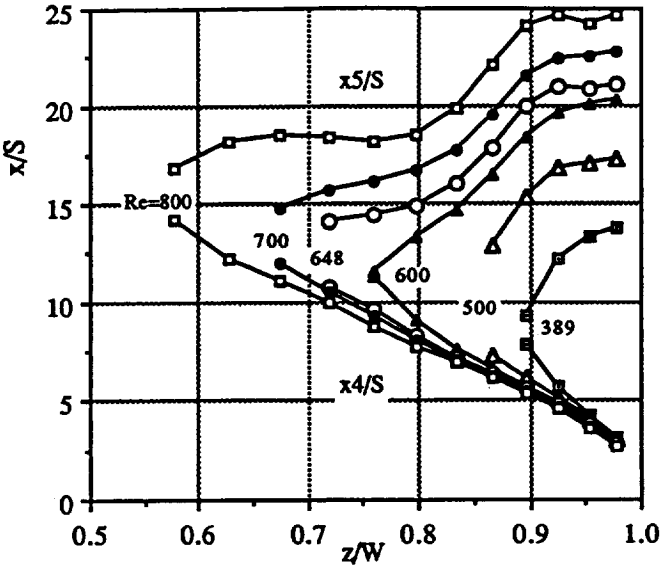

Figure 18. Spanwise distributions of detachment and reattachment length for various Reynolds numbers.

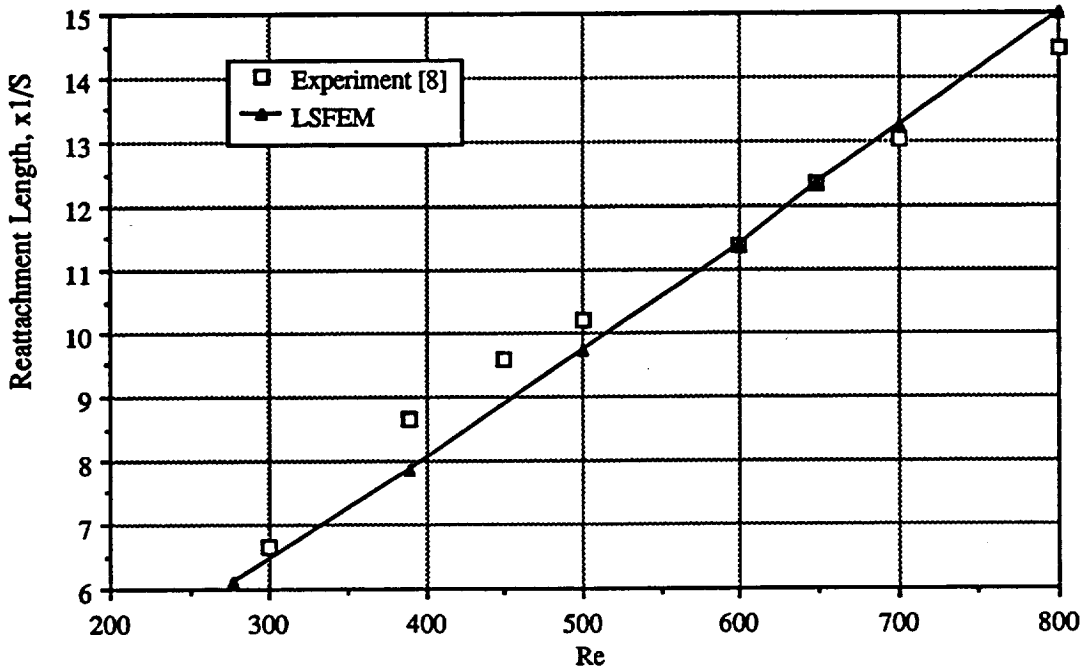

Figure 17. Comparison of experimental and simulation results for primary reattachment length up to Re=800.

REPORT DOCUMENTATION PAGE

Form Approved
OMB No. 0704-0188

1. AGENCY USE ONLY (*Leave blank*)	2. REPORT DATE	3. REPORT TYPE AND DATES COVERED
	August 1993	Technical Memorandum

4. TITLE AND SUBTITLE

Least-Squares Finite Element Solutions for Three-Dimensional Backward-Facing Step Flow

5. FUNDING NUMBERS

WU-505-90-5K

6. AUTHOR(S)

Bo-Nan Jiang, Lin-Jun Hou and Tsung-Liang Lin

7. PERFORMING ORGANIZATION NAME(S) AND ADDRESS(ES)

National Aeronautics and Space Administration
Lewis Research Center
Cleveland, Ohio 44135-3191

8. PERFORMING ORGANIZATION REPORT NUMBER

E-8136

9. SPONSORING/MONITORING AGENCY NAME(S) AND ADDRESS(ES)

National Aeronautics and Space Administration
Washington, D.C. 20546-0001

10. SPONSORING/MONITORING AGENCY REPORT NUMBER

NASA TM-106353
ICOMP-93-31

11. SUPPLEMENTARY NOTES

Prepared for the Fifth International Symposium on Computational Fluid Dynamics, Sendai, Japan, August 31- September 3, 1993. Bo-Nan Jiang and Lin-Jun Hou, Institute for Computational Mechanics in Propulsion, NASA Lewis Research Center and Tsung-Liang Lin, Livermore Software Technology Corporation, Livermore, California, 94550 (work funded under NASA Cooperative Agreement NCC3-233). ICOMP Program Director, Louis A. Povinelli, (216) 433-5818.

12a. DISTRIBUTION/AVAILABILITY STATEMENT

Unclassified - Unlimited
Subject Category 64

12b. DISTRIBUTION CODE

13. ABSTRACT (*Maximum 200 words*)

Comprehensive numerical solutions of the steady state incompressible viscous flow over a three-dimensional backward-facing step up to $Re = 800$ are presented. The results are obtained by the least-squares finite element method (LSFEM) which is based on the velocity-pressure-vorticity formulation. The computed model is of the same size as that of Armaly's experiment. Three-dimensional phenomena are observed even at low Reynolds number. The calculated values of the primary reattachment length are in good agreement with experimental results.

14. SUBJECT TERMS

Least squares; Finite element; Jacobi preconditional conjugate gradient method; Three-dimensional backward facing step flow

15. NUMBER OF PAGES

22

16. PRICE CODE

A03

17. SECURITY CLASSIFICATION OF REPORT	18. SECURITY CLASSIFICATION OF THIS PAGE	19. SECURITY CLASSIFICATION OF ABSTRACT	20. LIMITATION OF ABSTRACT
Unclassified	Unclassified	Unclassified	